Economic constrained optimization for power balancing in a DC microgrid: A multi-source elevator system application

Thanh Hung Pham, Ionela Prodan, Denis Genon-Catalot, Laurent Lefèvre

Economic constrained optimization for power balancing in a DC microgrid: a multi-source elevator system application

Thanh Hung Pham, Ionela Prodan, Denis Genon-Catalot, and Laurent Lefèvre

Univ. Grenoble Alpes, Grenoble INP, LCIS, F-26000 Valence, France*
** Institute of Engineering Univ. Grenoble Alpes*

Abstract

This paper considers a discrete-time scheduling method for the power balancing of a continuous-time DC microgrid system. A high-order dynamics and a resistor network are used for modelling the electrical storage unit and the DC bus of the centralized microgrid system, respectively. A PH (Port-Hamiltonian) formulation on graphs is employed to explicitly describe the microgrid topology. This modelling approach allows us to derive a discrete-time model which preserves the power and energy balance of the physical system. Next, a constrained economic MPC (Model Predictive Control) using the proposed control model is formulated for efficiently managing the microgrid operation. The systematic combination of the network modelling method and optimization-based control allows us to generate the appropriate power profiles. Finally, the benefits of the proposed approach are validated through simulation and comparison results over a particular DC microgrid elevator system under different scenarios and using real numerical data.

Keywords: DC microgrid, Port-Hamiltonian systems on graphs, Model Predictive Control

1. Introduction

Nowadays, industrial and research communities are concentrating their attention to microgrid systems and their development for improving the energy reliability of the classical power grid. A microgrid is represented by a group of interconnected customer loads and Distributed Energy Resources (DER) within clearly defined electrical boundaries which acts as a single controllable entity that can connect and disconnect from the grid (known as "islanding") [1].

DERs are small power sources that can be aggregated to provide the power necessary to meet (part of) a regular demand. It includes the distributed energy storage and generation systems. The distributed energy generation systems are integrated to the local system to reduce the impact on the environment of the fossil fuel resources. However, the electricity price of the external grid varies during a day. It may be expensive when the energy demand is high. Moreover, the power supplied by the distributed energy generation system is unstable [2, 3]. Consequently, the distributed energy storage system is used to store energy when it is available and cheap. Then, it is reused in the contrary case. In microgrids, DERs are connected to the load systems through converters to satisfy the energy demand [4, 5].

We focus here on DC microgrid systems (e.g., the multi-source elevator system described in Fig. 1) due to their ability to integrate (through DC/DC or AC/DC converters) different distributed renewable energy resources which generate DC power (e.g., the solar panel) or AC power with varying frequencies (e.g., wind turbine). Nonetheless, DC to AC converters are still necessary due to the fact that some sources and loads cannot be directly connected to the DC bus.

Within the global energy system the fast dynamics correspond to the actuators (e.g., converter, motor), transmission lines and high power energy storage (e.g., supercapacitor) which need to be stabilized around a set-point (see, e.g, [6, 7]). The slow dynamics correspond to the energy storage unit (e.g., battery, elevator system, thermal system) and are governed by cost criteria [8, 9]. Thus, at the control design step we need to take into account the different timescales appearing in the system dynamics. With respect to the above mentioned issues, let us delineate the following remarks:

- The energy cost optimization is generally a continuous-time optimization problem for which the solution gives the time profile of the control variables. Usually, it is difficult to find its exact solution. In this work, we consider the indirect approach where we discretize the optimization problem to obtain a finite-dimensional optimization problem which is easier to solve (the reader is referred to [10] for details on the direct and indirect approaches). Moreover, its discretization requires the discrete-time model of the microgrid dynamics.

- The microgrid dynamics has different time scales [11]. To reduce the computational complexity, the energy cost optimization usually uses the slow dynamics ob-

tained by reducing the fast dynamics of the converter and the transmission lines.

The excess power of a distributed system is usually evaluated by selling to the external grid or storing in an electrical storage system. Hence, the storage scheduling is an important issue, knowing the fact that the storage capacity (i.e., power and energy) is limited. The authors of [1, 12] proposed a reactive method (without considering prediction) based on logical rules to switch the system to different operation modes. To reduce the required computation and increase the robustness, this method is formulated in [13] through the use of multi-agent systems paradigm. However, this approach is not efficient since, in some cases, the battery can charge from the external grid when the electricity price is expensive. An off-line optimization-based control approach which takes into account the system dynamics, constraints and power prediction is proposed in [14, 15]. However, to improve the control design robustness, some works concentrate on its on-line version, i.e., MPC (Model Predictive Control) (see, e.g., [16]). Note that there are two types of MPC: tracking MPC [17, 18] and economic MPC [19, 20]. The tracking MPC aims at stabilizing the systems to given references by penalizing in the cost function the discrepancies between controlled variables and their references. Moreover, for the effectiveness, chosen cost functions are usually convex which are minimal on the corresponding reference profiles. In economic MPC, the cost functions reflect profit criteria which are generally nonlinear and non-convex. Moreover, this controller is used to generate references for lower levels regulators. Thus, the MPC for minimizing the electricity cost of microgrid systems can be categorized into economic MPC [9].

The authors in [8, 21] use in an MPC framework simple models for the battery and/or transmission lines which do not entirely capture the real dynamics properties. They use a first-order model for the electrical storage unit. In fact, the electrical storage unit (e.g., a battery) may include many sub-storage parts which are connected by resistive elements. Only some of these parts can directly supply the energy. For the slow time scale, the internal charge distribution between these parts can not be ignored. Thus, a first-order model for the electrical storage unit may give incorrect informations about the real available charge. Also, in these works, the transmission lines network dynamics are simply described by a power balance relation. This is not realistic for DC microgrids where the components are placed far from the each other [4]. Hence, the resistance of the transmission lines can not be neglected.

In general, the microgrid dynamics has at least two energetic properties which may be useful for studying the energy cost optimization: the energy balance and the underlying power-preserving structure. For example, [9, 22] and many other works do not take explicitly into account these properties when developing the model of the microgrid system. Thus, the properties may be lost while studying the energy cost optimization through the model discretization and reduction. To preserve these energetic properties, we employ a modelling approach using the Port-Hamiltonian formulation where the system power-preserving interconnection and the stored energy are explicitly described [23]. The PH formalism is useful for the system stability analysis and for the control design based on the interconnection, dissipation and stored energy of the system dynamics. An interesting property of PH systems is the passivity where the energy (Hamiltonian) is considered as a Lyapunov function. There are many control methods developed for the PH systems as presented in [23], e.g., Control by Interconnection, Interconnection and Damping Assignment Passivity-Based Control (IDA PBC). None of these methods can explicitly deal with state and input constraints. MPC on the other hand can handle them successfully. While the theory on linear MPC gained ground over the last decades, the non linear and economic MPC are still under active research due to theoretical and practical issues. For example, stability demonstration for the closed-loop nonlinear system is difficult since a Lyapunov function is not easy to find. From the previous arguments, while both PH formalism and MPC are established tools in the literature, to the best of our knowledge they have never been considered together by the control community.

The present paper extends the work of the authors proposed in [24] where a discrete-time economic MPC for power balancing in a continuous DC microgrid is proposed. More specifically, this work includes the following contributions:

- A PH formulation which completely describes the power interconnection of the DC microgrid components is developed. Moreover, the PH representation on graphs (see also [25]) allows us to explicitly capture the topology of the electrical circuit. It is simplified to the classical hybrid input-output representation of the microgrid network associated with constraints. Using the latter formulation we reduce the variable number and the optimization complexity while preserving the system topology.
- A discrete-time model preserving the power and energy balance is derived.
- A centralized economic MPC design for battery scheduling is developed taking into account the global discrete time model of the system, constraints and electricity cost minimization.
- Extensive simulation and comparison scenarios are implemented. The results illustrate the increasing electricity cost profit by increasing the DERs dimensions, the robustness of the control method and its economic efficiency with respect to other control formulations.

This paper is organized as follows. Section 2 details some basic notion on PH systems on graphs. Section 3

introduces the DC microgrid model and the constraints. Next, Section 4 formulates the online constrained optimization problem for reliable battery scheduling. Section 5 details the simulation result under different scenarios. Finally, Section 6 draws the conclusions and presents the future work.

Notation

This subsection presents the important notations used throughout the paper.

Table 1: Notations and fonts for the parameters and the variables.

Notation	Description
$(.)(t)$	continuous-time function $(.)$
$\dot{(.)}(t)$	time derivative of $(.)(t)$
$(.)(j)$	discrete-time function $(.)$
$\overline{(.)}(t)$	reference value of $(.)(t)$
$(.)(t+\tau\|t)$	denotes the value of $(.)$ at time instant $t+\tau$, predicted upon the information available at time $t \in \mathbf{N}$.
H	Hamiltonian function
$\partial_x H(\mathbf{x})$	partial derivative of H with respect to x
$\nabla H(\mathbf{x})$	gradient of $H(\mathbf{x})$
i, v	current and voltage
x	state variable
P	power
R	resistor
q_{max}	maximal battery charge
d	duty cycle
h	time step
α, β	ratios between the real and reference values
$\mathbf{B}$	incidence matrix
$\mathbf{Q}$	weight matrix of the Hamiltonian
$\mathbf{1}_n$	vector of n entries 1
$\mathbf{I}_n$	identity matrix of dimension n
$\mathbf{0}_{n\times m}$	matrix of all entries 0 with size of $n \times m$

Element	Font
Scalar parameter	Capital letter
Scalar variable	Normal letter
Vector	Normal and bold letter
Matrix	Capital and bold letter
Set	Capital and blackboard bold letter

2. Preliminaries

In this section, we present the PH systems on graphs and the MPC formulation which will be further used to express the power balancing problem.

2.1. Port-Hamiltonian systems on graphs

This subsection briefly introduces some basic definitions and notions related to PH systems on graphs, which will be further used for modelling the DC network (for more details the reader is referred to [25]).

Definition 2.1. *[Directed (closed) graph, [25]] A directed graph $\mathbb{G} = (\mathbb{V}, \mathbb{E})$ consists of a finite set $\mathbb{V}$ of N_v vertices, a finite set $\mathbb{E}$ of N_e directed edges, together with a mapping from $\mathbb{E}$ to the set of ordered pairs of $\mathbb{V}$, where no self-loops*

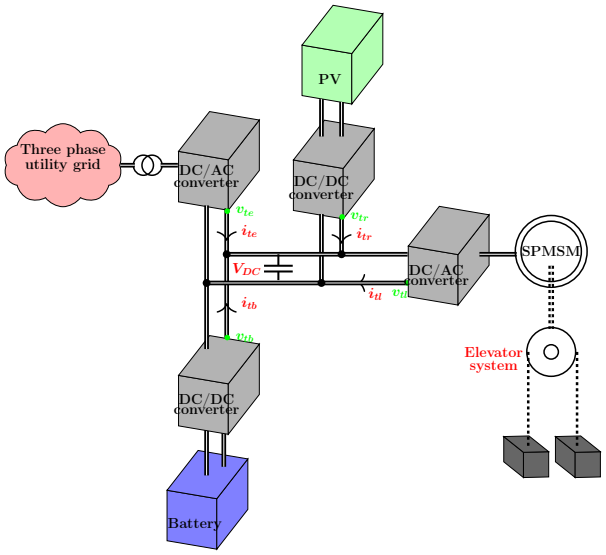

Figure 1: DC microgrid elevator system.

are allowed. The incidence matrix $\mathbf{B} \in \mathbb{R}^{N_v \times N_e}$ describes the map from $\mathbb{E}$ to $\mathbb{V}$ such that:

$$\mathbf{B}_{ij} = \begin{cases} 1, & \text{if node } i \text{ is a head vertex of edge } j, \\ -1, & \text{if node } i \text{ is a end vertex of edge } j, \\ 0, & \text{else.} \end{cases} \quad (1)$$

Next, the graph notion is used to define the Kirchhoff-Dirac (KD) structure of a DC circuit $\mathbb{G}$ of N_v nodes and N_e edges.

Definition 2.2. *[KD structure on graphs, [25]] The KD structure on graphs is defined as:*

$$\begin{aligned} \mathbb{D}(\mathbb{G}) = \{(\mathbf{i}, \mathbf{v}) \in \mathbb{R}^{N_e} \times \mathbb{R}^{N_e} | \\ \mathbf{B}\mathbf{i} = \mathbf{0},\ \exists \mathbf{v}_p \in \mathbb{R}^{N_v} \text{ such that } \mathbf{v} = -\mathbf{B}^T \mathbf{v}_p\}, \end{aligned} \quad (2)$$

where $\mathbf{B}$ is the incidence matrix of the electrical circuit graph $\mathbb{G}$ as defined in (1), $\mathbf{v}_p \in \mathbb{R}^{N_v}$ denotes the node potential, $\mathbf{v} \in \mathbb{R}^{N_e}$ denotes the edge voltage and $\mathbf{i} \in \mathbb{R}^{N_e}$ denotes the edge current.

To formulate the PH systems, N_e edge ports $(\mathbf{i}, \mathbf{v})$ as in Definition (2.2) are partitioned into N_S energy storage ports $(\mathbf{i}_S, \mathbf{v}_S)$, N_R resistive ports $(\mathbf{i}_R, \mathbf{v}_R)$ and N_E external ports $(\mathbf{i}_E, \mathbf{v}_E)$.

Definition 2.3. *[PH systems on graphs, [25]] Consider a state space $\mathbb{X}$ with its tangent space $T_x\mathbb{X}$, co-tangent space $T_x^*\mathbb{X}$, and a Hamiltonian $H : \mathbb{X} \to \mathbb{R}$, defining the energy-storage. A PH system of KD structure $\mathbb{D}(\mathbb{G})$ on $\mathbb{X}$ is defined by a Dirac structure $\mathbb{D}(\mathbb{G}) \subset T_x\mathbb{X} \times T_x^*\mathbb{X} \times \mathbb{R}^{N_R} \times \mathbb{R}^{N_R} \times \mathbb{R}^{N_E} \times \mathbb{R}^{N_E}$ having energy-storing port $(\mathbf{i}_S, \mathbf{v}_S) \in T_x\mathbb{X} \times T_x^*\mathbb{X}$, a resistive structure*

$$\mathbb{R} = \left\{ (\mathbf{i}_R, \mathbf{v}_R) \in \mathbb{R}^{N_R} \times \mathbb{R}^{N_R} \,\middle|\, r(\mathbf{i}_R, \mathbf{v}_R) = 0,\ \mathbf{i}_R^T \mathbf{v}_R \leq 0 \right\},$$

and the external ports $(\mathbf{i}_E, \mathbf{v}_E) \in \mathbb{R}^{N_E} \times \mathbb{R}^{N_E}$. *Generally, the PH dynamics are described by*

$$(-\dot{\mathbf{x}}(t), \nabla H(\mathbf{x}), \mathbf{i}_R(t), \mathbf{v}_R(t), \mathbf{i}_E(t), \mathbf{v}_E(t)) \in \mathbb{D}(\mathbb{G}).$$

2.2. Brief overview of Model Predictive Control

This subsection recalls the general formulation of MPC (Model Predictive Control) which will be used for the energy management problem formulation within the microgrid (for more details the reader is referred to [18]). Let $\mathbf{x}(t+h) = \mathbf{g}(t, \mathbf{x}(t), \mathbf{u}(t))$ be a discrete-time dynamical system, where t is the time instant, h is the time step, $\mathbf{x}(t) \in \mathbb{X}(t)$ is the state vector, and $\mathbf{u}(t) \in \mathbb{U}(t)$ is the control vector. We denote the predicted values of the variables at instant $t+jh$ by $\mathbf{x}(j|t)$, $\mathbf{u}(j|t)$ with $j \in \mathbb{N}$. We consider the recursive construction of an optimal open-loop state and control sequences:

$$\begin{aligned} \mathbf{X}(t) &\triangleq \{\mathbf{x}(0|t), \ldots, \mathbf{x}(j|t), \ldots, \mathbf{x}(N_p-1|t), \mathbf{x}(N_p|t)\}, \\ \mathbf{U}(t) &\triangleq \{\mathbf{u}(0|t), \ldots, \mathbf{u}(j|t), \ldots, \mathbf{u}(N_p-1|t)\} \end{aligned}$$

at instant t over a finite receding horizon, N_p, which leads to a feedback control policy by the effective application of the first control action as system input:

$$\mathbf{u}(t|t) = \underset{\mathbf{U}(t)}{\operatorname{argmin}} \left[V_f(t, \mathbf{x}(N_p|t)) + \sum_{j=0}^{N_p-1} V_r(t+jh, \mathbf{x}(j|t), \mathbf{u}(j|t)) \right]$$

subject to

$$\begin{aligned} \mathbf{x}(j+1|t) &= \mathbf{g}(t+jh, \mathbf{x}(j|t), \mathbf{u}(j|t)), \\ \mathbf{x}(0|t) &= \mathbf{x}(t), \\ \mathbf{x}(j+1|t) &\in \mathbb{X}(t+(j+1)h), \\ \mathbf{u}(j|t) &\in \mathbb{U}(t+jh), \\ \mathbf{x}(N_p|t) &\in \mathbb{X}_f(t), \end{aligned}$$

where $j = 0, \ldots, N_p-1$. $V_f(t, \mathbf{x}(t))$, $V_r(t, \mathbf{x}(t), \mathbf{u}(t))$, $\mathbb{X}_f(t)$ are the final cost, the running cost and the final set, respectively, which are also the tuning control parameters.

3. DC microgrid model

This section describes in detail the model of the DC microgrid elevator system illustrated in Fig. 1. The system is equivalently represented by the electrical DC circuit in Fig 2 where we denote at the circuit node 1 the common ground.

3.1. Components models and constraints

3.1.1. External grid:

As illustrated in Fig. 2 the DC microgrid is connected to the AC external grid which is modeled here as a controllable current source $i_e(t) \in \mathbb{R}$ with the following physical limitations:

$$i_{e,min} \leq i_e(t) \leq i_{e,max}, \tag{3}$$

with the upper and lower bounds $i_{e,max}, i_{e,min} \in \mathbb{R}$.

3.1.2. Load unit:

The load component of the DC microgrid represents a combination of the electromechanical elevator and an AC/DC converter. Here, we simply model this as a power source $P_l(t) \in \mathbb{R}$ under current, $i_l(t) \in \mathbb{R}$, and voltage, $v_l(t) \in \mathbb{R}$, constraint:

$$i_l(t) v_l(t) = -P_l(t). \tag{4}$$

3.1.3. Renewable source:

The DC microgrid system contains a solar panel and the corresponding DC/DC converter. Similarly, we model the distributed energy resource as a power source $P_r(t) \in \mathbb{R}$ satisfying the following relation:

$$i_r(t) v_r(t) = P_r(t), \tag{5}$$

with $i_r(t), v_r(t) \in \mathbb{R}$ the renewable source current and voltage as illustrated in Fig. 2.

3.1.4. Electrical storage unit:

We consider here a lead-acid type of battery which is modelled as two electronic "wells", a bridge connecting them described by R_1 and an internal resistor R_2 (see also Fig. 2) [26, 27]. Therefore, hereinafter, we denote by $\mathbf{x}(t) \in \mathbb{R}^2$ the battery charges. The Hamiltonian representing the stored energy in the battery is given by:

$$H(\mathbf{x}) = \mathbf{x}(t)^T \mathbf{Q}_1 + \frac{1}{2} \mathbf{x}(t)^T \mathbf{Q}_2 \mathbf{x}(t), \tag{6}$$

with $\mathbf{Q}_1 = E\mathbf{1}_2 \in \mathbb{R}^2$, $\mathbf{Q}_2 = diag\{C_1, C_2\} \in \mathbb{R}^{2\times 2}$. E is the battery internal voltage; C_1 and C_2 are the battery internal capacitances. Usually, each battery has some limitations on the quantity of charged energy. Furthermore, the battery stored charge must be greater than half its capacity (kept in case of unexpected events):

$$\alpha_{min} \mathbf{x}_{max} \leq \mathbf{x}(t) \leq \alpha_{max} \mathbf{x}_{max}, \tag{7}$$

with $\mathbf{x}_{max} \in \mathbb{R}^2$, α_{min} and α_{max} are appropriate coefficients such that $0 < \alpha_{min} < \alpha_{max} < 1$. In the one-dimension model of the battery ([28]), the maximum charge $q_{max} \in \mathbb{R}$ is derived from $\mathbf{x}_{max}$ by the relation:

$$q_{max} = \mathbf{1}_2^T \mathbf{x}_{max}. \tag{8}$$

Furthermore, the battery charge/ discharge current (equal to the current of internal resistor $i_{b,R2}(t)$) respects some limitation range given by the manufacturer.

$$i_{b,min} \leq i_{b,R2}(t) \leq i_{b,max}, \tag{9}$$

with $i_{b,min}$, $i_{b,max} \in \mathbb{R}$. Since this limitation of the battery current is valid for both charge and discharge modes of the battery operation, $i_{b,min}$ is considered negative, and $i_{b,max}$ is considered positive. Moreover, the maximum discharge current is usually greater than the maximum charge current, i.e., $-i_{b,min} > i_{b,max}$.

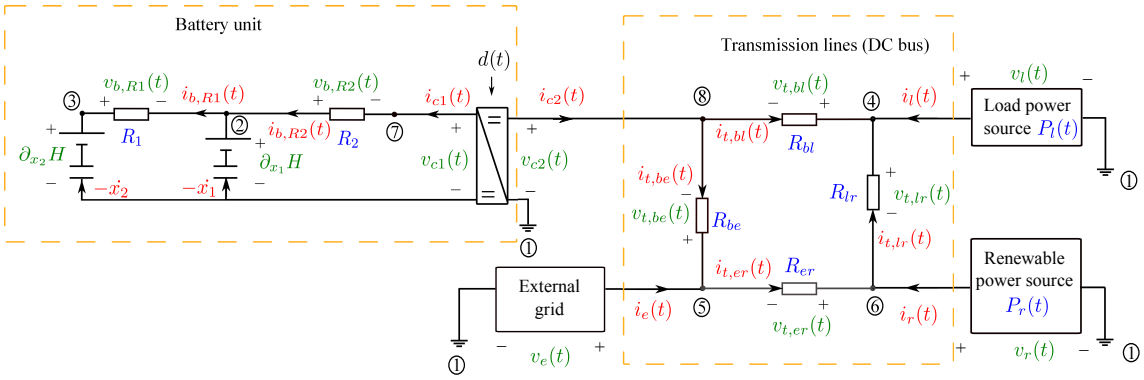

Figure 2: Electrical circuit of the DC microgrid.

Using the classical physics theory, the Ohm's law, we derive the current and voltage relation for the battery resistors:

$$\mathbf{R}_b \mathbf{i}_{bR}(t) + \mathbf{v}_{bR}(t) = \mathbf{0}, \tag{10}$$

with

$$\mathbf{i}_{bR}(t) = \begin{bmatrix} i_{b,R1}(t) \\ i_{b,R2}(t) \end{bmatrix}, \ \mathbf{v}_{bR}(t) = \begin{bmatrix} v_{b,R1}(t) \\ v_{b,R2}(t) \end{bmatrix} \in \mathbb{R}^2, \tag{11}$$

and $\mathbf{R}_b = diag\{R_1, R_2\} \in \mathbb{R}^{2\times 2}$ a positive diagonal matrix (see also Fig. 2).

3.1.5. The DC/DC converter:

As illustrated in Fig. 2, the battery has an associated DC/DC converter which is assumed to be an ideal transformer described by the following relations:

$$\begin{cases} d(t) i_{c1}(t) &= -i_{c2}(t), \\ v_{c1}(t) &= d(t) v_{c2}(t), \end{cases} \tag{12}$$

where $d(t) \in \mathbb{R}$ represents the positive duty cycle:

$$d(t) > 0. \tag{13}$$

While in the rest of the paper we assume no loss at charge/discharge in the DC/DC converter for simplicity, non zero charge/discharge losses can be taken into account by the resistor series connections to the two sides of the converter in Fig. 2 with appropriate values. These additional resistors are, then, fused with the resistors of the battery or the DC bus. Consequently, with suitable resistor values of the battery and/or the DC bus, the electrical circuit of the DC microgrid in Fig. 2 is still valid.

3.1.6. Transmission lines and resistor network:

The DC bus, i.e., the transmission lines, are illustrated in the electrical circuit of Fig. 2. It is modeled, in general, as a capacitor connected in parallel with the power units ([29]). In a large DC microgrid, the capacitor, inductor and resistor cannot be neglected [30]. However, in the forthcoming scheduling problem, the DC bus dynamics is stabilized, that is, its capacitors and inductors are eliminated. Thus, the DC bus model is reduced to a resistor network (see [31]). Using the classical physics theory, the Ohm's law, we derive the current and voltage relation for the resistor network:

$$\mathbf{R}_t \mathbf{i}_{tR}(t) + \mathbf{v}_{tR}(t) = \mathbf{0}, \tag{14}$$

with

$$\begin{aligned} \mathbf{i}_{tR}(t) &= [i_{t,bl}(t) \ \ i_{t,be}(t) \ \ i_{t,er}(t) \ \ i_{b,rl}(t)]^T \quad \in \mathbb{R}^4, \\ \mathbf{v}_{tR}(t) &= [v_{t,bl}(t) \ \ v_{t,be}(t) \ \ v_{t,er}(t) \ \ v_{t,rl}(t)]^T \quad \in \mathbb{R}^4, \end{aligned} \tag{15}$$

and $\mathbf{R}_t = diag\{R_{bl}, R_{be}, R_{er}, R_{lr}\} \in \mathbb{R}^{4\times 4}$ a positive diagonal matrix (see also Fig. 2).

Next, using the definition of the KD structure in (2) we present the interconnections of the DC microgrid network through a closed graph.

3.2. DC microgrid network

The microgrid network includes all the elements enumerated above, the battery charges, the load, the renewable source, the external grid, the DC/DC converter and the resistor network of the DC bus.

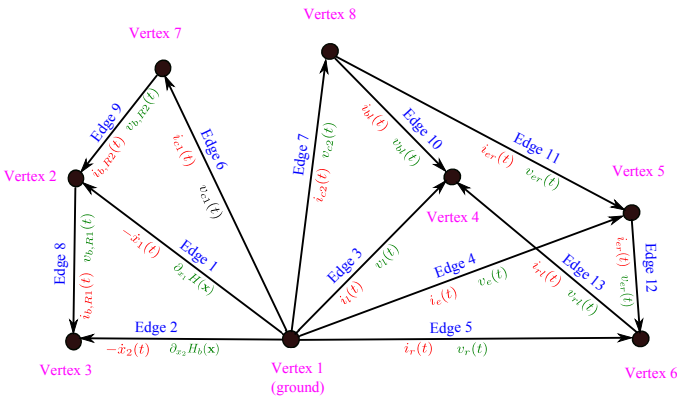

Figure 3: Directed graph corresponding to the DC microgrid circuit.

The edge current and voltage vectors, $\mathbf{i}(t), \mathbf{v}(t) \in \mathbb{R}^{13}$, are denoted by:

$$\begin{cases} \mathbf{i}(t) &= [-\dot{\mathbf{x}}^T(t) \;\; i_{c1}(t) \;\; \mathbf{i}_E^T(t) \;\; \mathbf{i}_{bR}^T(t) \;\; \mathbf{i}_{tR}^T(t)]^T, \\ \mathbf{v}(t) &= [\nabla H^T(t) \;\; v_{c1}(t) \;\; \mathbf{v}_E^T(t) \;\; \mathbf{v}_{bR}^T(t) \;\; \mathbf{v}_{tR}^T(t)]^T, \end{cases} \tag{16}$$

where

$$\begin{cases} \mathbf{i}_E(t) &= [i_{c2}(t) \;\; i_l(t) \;\; i_e(t) \;\; i_r(t)]^T \quad \in \mathbb{R}^4, \\ \mathbf{v}_E(t) &= [v_{c2}(t) \;\; v_l(t) \;\; v_e(t) \;\; v_r(t)]^T \quad \in \mathbb{R}^4, \end{cases} \tag{17}$$

gathers the currents and voltages of the load, the external grid and the renewable source, respectively. As illustrated in Fig. 2, we consider node 1 as the circuit "ground" node of the DC microgrid hence, its potential is set to zero:

$$v_{p1}(t) = 0, \tag{18}$$

and used as reference for measuring the potential at the other nodes in the circuit denoted by $\mathbf{v}_p(t) = [v_{p1}(t) \; \mathbf{v}_{p2}^T(t)]^T$ with $\mathbf{v}_{p2}(t) \in \mathbb{R}^7$. From the Definition 2.2, the Kirchhoff-Dirac structure of the microgrid network is described as:

$$\begin{cases} \mathbf{v}(t) = & -\mathbf{B}^T \mathbf{v}_p(t), \\ \mathbf{0} = & \mathbf{B}\mathbf{i}(t), \end{cases} \tag{19}$$

where $\mathbf{B} \in \mathbb{R}^{8\times 13}$ is the incidence matrix defined in (1):

$$\mathbf{B} = \begin{bmatrix} \mathbf{1}_7^T & \mathbf{0} \\ -\mathbf{I}_7 & \mathbf{B}_{22} \end{bmatrix}, \tag{20}$$

with $\mathbf{B}_{22} \in \mathbb{R}^{7\times 6}$ describing the interconnection of the resistor network:

$$\mathbf{B}_{22} = \begin{bmatrix} 1 & -1 & 0 & 0 & 0 & 0 \\ -1 & 0 & 0 & 0 & 0 & 0 \\ 0 & 1 & 0 & 0 & 0 & 0 \\ 0 & 0 & 1 & 1 & 0 & 0 \\ 0 & 0 & -1 & 0 & 0 & -1 \\ 0 & 0 & 0 & -1 & 1 & 0 \\ 0 & 0 & 0 & 0 & -1 & 1 \end{bmatrix}. \tag{21}$$

By considering the incidence matrix form in (20), we simplify the algebraic equations in (19) and eliminate the node potential vector, $\mathbf{v}_p(t)$. Let the edge current and voltage vectors, $\mathbf{i}(t)$ and $\mathbf{v}(t)$, defined in (16) be partitioned into the vectors $\mathbf{i}_1(t) \in \mathbb{R}^7$, $\mathbf{i}_2(t) \in \mathbb{R}^6$, $\mathbf{v}_1(t) \in \mathbb{R}^7$ and $\mathbf{v}_2(t) \in \mathbb{R}^6$ such as:

$$\begin{cases} \mathbf{i}_1(t) = & [\; -\dot{\mathbf{x}}^T(t) \quad i_{c1}(t) \quad \mathbf{i}_E^T(t) \;]^T, \\ \mathbf{v}_1(t) = & [\; \nabla H^T(t) \quad v_{c1}(t) \quad \mathbf{v}_E^T(t) \;]^T, \\ \mathbf{i}_2(t) = & [\; \mathbf{i}_{bR}^T(t) \quad \mathbf{i}_{tR}^T(t) \;]^T, \\ \mathbf{v}_2(t) = & [\; \mathbf{v}_{bR}^T(t) \quad \mathbf{v}_{tR}^T(t) \;]^T. \end{cases} \tag{22}$$

Note that $\mathbf{i}_1(t)$, $\mathbf{v}_1(t)$ describe the currents and voltages of the battery capacitors, the energy sources and the converter. Next, $\mathbf{i}_2(t)$, $\mathbf{v}_2(t)$ describe the currents and voltages of the circuit resistors. From (18), (19)-(22), the microgrid network described in (19)-(21) is rewritten as:

$$\begin{bmatrix} \mathbf{i}_1(t) \\ \mathbf{v}_2(t) \end{bmatrix} = \begin{bmatrix} \mathbf{0} & \mathbf{B}_{22} \\ -\mathbf{B}_{22}^T & \mathbf{0} \end{bmatrix} \begin{bmatrix} \mathbf{v}_1(t) \\ \mathbf{i}_2(t) \end{bmatrix}, \tag{23}$$

where $\mathbf{i}_1(t)$, $\mathbf{v}_1(t)$, $\mathbf{i}_2(t)$, $\mathbf{v}_2(t)$ are defined in (22). Note that the equations (23) imply the power-preserving property of the microgrid network thanks to the skew-symmetric form of the interconnection matrix.

Remark 3.1. *As we can see in* (21)*, matrix* $\mathbf{B}_{22}$ *has the following form:*

$$\mathbf{B}_{22} = \begin{bmatrix} \mathbf{B}_b & \mathbf{0}_{3\times 4} \\ \mathbf{0}_{4\times 2} & \mathbf{B}_t \end{bmatrix}, \tag{24}$$

where the matrices $\mathbf{B}_b \in \mathbb{R}^{3\times 2}$ *and* $\mathbf{B}_t \in \mathbb{R}^{4\times 4}$ *represent the structure of the battery and the transmission lines. Thus, for describing the structure of a more complex microgrid where many electricity storage units and power sources are used, we independently add other blocks* $\mathbf{B}_b$ *and modify matrix* $\mathbf{B}_t$ *with corresponding sizes.*

Next, we introduce the microgrid dynamics which characterizes the centralized system.

3.3. Global DC microgrid model

Combining the above relations (4)-(6), (10), (12), (14), (22) and (23) we formulate the global microgrid model:

$$\begin{bmatrix} \mathbf{i}_1(t) \\ \mathbf{v}_2(t) \end{bmatrix} = \begin{bmatrix} \mathbf{0} & \mathbf{B}_{22} \\ -\mathbf{B}_{22}^T & \mathbf{0} \end{bmatrix} \begin{bmatrix} \mathbf{v}_1(t) \\ \mathbf{i}_2(t) \end{bmatrix}, \tag{25a}$$

$$\begin{bmatrix} v_{c1}(t) \\ i_{c2}(t) \end{bmatrix} = \begin{bmatrix} 0 & -d(t) \\ d(t) & 0 \end{bmatrix} \begin{bmatrix} i_{c1}(t) \\ v_{c2}(t) \end{bmatrix}, \tag{25b}$$

$$i_r(t)v_r(t) = \; P_r(t), \tag{25c}$$

$$i_l(t)v_l(t) = -\, P_l(t), \tag{25d}$$

$$\mathbf{v}_{bR}(t) = -\, \mathbf{R}_b \mathbf{i}_{bR}(t), \tag{25e}$$

$$\mathbf{v}_{tR}(t) = -\, \mathbf{R}_t \mathbf{i}_{tR}(t), \tag{25f}$$

where $\mathbf{i}_1(t)$, $\mathbf{v}_1(t) \in \mathbb{R}^7$ gather the current and voltage variables of the microgrid components, $\mathbf{i}_2(t)$, $\mathbf{v}_2(t) \in \mathbb{R}^6$ gather the current and voltage variables of the resistors of the battery and of the transmission lines (see also (22)). Also, in (25), $i_{c1}(t)$, $i_{c2}(t)$, $v_{c1}(t)$, $v_{c2}(t) \in \mathbb{R}$ are the current and voltage variables at the two sides of the DC/DC converter (see also (12)), $i_r(t)$, $v_r(t) \in \mathbb{R}$ are the current and voltage variables of the renewable source, $i_l(t)$, $v_l(t) \in \mathbb{R}$ are the current and voltage variables of the load (i.e., the electro-mechanical elevator). Furthermore, $d(t) \in \mathbb{R}$ is the converter duty cycle, $\mathbf{B}_{22} \in \mathbb{R}^{7\times 6}$ is the structure matrix defined in (21). Next, $\mathbf{i}_{bR}(t)$, $\mathbf{v}_{bR}(t) \in \mathbb{R}^2$ are the current and voltage variables of the battery resistors in (11), $\mathbf{i}_{tR}(t)$, $\mathbf{v}_{tR}(t) \in \mathbb{R}^4$ are the current and voltage variables of the transmission line resistors in (15). $\mathbf{R}_b \in \mathbb{R}^{2\times 2}$, $\mathbf{R}_t \in \mathbb{R}^{4\times 4}$ are the resistive matrices of the battery and of the transmission lines in (11) and (15), respectively.

Remark 3.2. *The transmission line resistances* $\mathbf{R}_t$ *in* (14) *can be easily measured. The battery parameters* $\mathbf{R}_b$, $\mathbf{Q}_1$ *and* $\mathbf{Q}_2$ *in* (10) *and* (6) *can be off-line determined through experimental identification [26].*

Remark 3.3. *The internal battery variables can be estimated using observers. Indeed, from* (10)-(11) *and* (21)-(23)*, we derive the battery dynamics:*

$$\begin{cases} \dot{x_1}(t) &= -\dfrac{1}{R_1C_1}x_1(t) + \dfrac{1}{R_1C_2}x_2(t), \\ \dot{x_2}(t) &= \dfrac{1}{R_1C_1}x_1(t) - \dfrac{1}{R_1C_2}x_2(t) + i_{c1}(t), \\ v_{c1}(t) &= E + \dfrac{1}{C_2}x_2(t) + R_2 i_{c1}(t). \end{cases} \quad (26)$$

It is easy to verify that system (26) *is observable (i.e., the observability matrix is full rank). This implies that, by using the battery current and voltage measurement with a suitable observer, we can estimate the battery charges, and thus, the other variables.*

3.4. Reference profiles

All the elements of the electrical system are characterized by certain profiles of reference. The following data profiles are taken from the industrial partner Sodimas (an elevator company from France) and illustrated in Fig. 4. Taking into account the available statistical measurements of electricity consumption we consider the reference power of the consumer denoted by $\overline{P_l}(t)$. Furthermore, we denote by $\overline{P_r}(t)$ the power profile of the renewable source estimated from meteorological data. Lastly, by using existing historical data of electricity market, we denote the predicted electricity price profile by $price(t)$. Moreover, we assume that the selling and buying prices are the same.

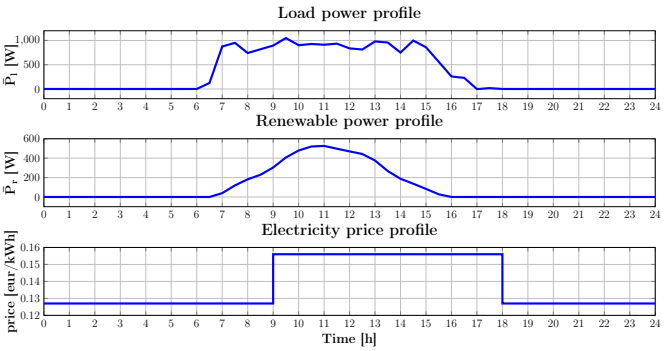

Figure 4: Profiles of load, renewable power and electricity price.

Having the centralized model, constraints and parameter profiles of the microgrid system we formulate in the forthcoming section the global optimal power balancing problem.

4. Battery scheduling by optimization-based control

In this section, the previously developed dynamics, constraints and profiles will be used in a discrete-time constrained optimization problem. Hence, we will first introduce the global discrete-time model of the DC microgrid which preserves the energy conservation properties of the continuous time model formulated in (6), (11), (15), (17), (21)-(22) and (25). The ultimate goal is to provide an efficient scheduling for the electrical storage such that cost and constraints are satisfied.

4.1. Energy-preserving discrete-time model

In general, when discretizing a continuous time system, the energy conservation property should always be taken into account. For a nonlinear PH system as in (6), (11), (15), (17), (21)-(22) and (25) this property can be ensured by preserving the KD structure (2) and the energy flowing through the storage ports (see also Fig. 5). Let $(.)(j)$ be the discrete value of variable $(.)(t)$ at time instant $t = t_0 + (j-1)h$ with the time step h and the initial time instant t_0. We define the discrete-time interconnection of the microgrid network illustrated in (23):

$$\begin{bmatrix} \mathbf{i}_1(j) \\ \mathbf{v}_2(j) \end{bmatrix} = \begin{bmatrix} \mathbf{0} & \mathbf{B}_{22} \\ -\mathbf{B}_{22}^T & \mathbf{0} \end{bmatrix} \begin{bmatrix} \mathbf{v}_1(j) \\ \mathbf{i}_2(j) \end{bmatrix}, \quad (27a)$$

$$\begin{bmatrix} v_{c1}(j) \\ i_{c2}(j) \end{bmatrix} = \begin{bmatrix} 0 & -d(j) \\ d(j) & 0 \end{bmatrix} \begin{bmatrix} i_{c1}(j) \\ v_{c2}(j) \end{bmatrix}, \quad (27b)$$

The discretizations of the load and of the renewable source are defined as:

$$i_l(j)v_l(j) = -P_l(j), \quad (28a)$$
$$i_r(j)v_r(j) = P_r(j), \quad (28b)$$

where the discrete-time power profiles, $P_l(j)$, $P_r(j)$, are the average values of the reference continuous-time power profiles, $\overline{P_l}(t)$, $\overline{P_r}(t)$ such that:

$$\begin{cases} P_l(j) &= \displaystyle\int_{(j-1)h}^{jh} \frac{\overline{P_l}(t)}{h} dt, \\ P_r(j) &= \displaystyle\int_{(j-1)h}^{jh} \frac{\overline{P_r}(t)}{h} dt, \end{cases} \quad (29)$$

The discrete-time Ohm's law for the battery and transmission lines resistors are defined as:

$$\mathbf{v}_{bR}(j) = -\mathbf{R}_b \mathbf{i}_{bR}(j), \quad (30a)$$
$$\mathbf{v}_{tR}(j) = -\mathbf{R}_t \mathbf{i}_{tR}(j), \quad (30b)$$

where the resistive matrices, $\mathbf{R}_b \in \mathbb{R}^{2\times 2}$, $\mathbf{R}_t \in \mathbb{R}^{4\times 4}$, are defined in (10) and (14).

Note that discretizations of the current and voltage vectors, $\mathbf{i}_1(t)$, $\mathbf{i}_2(t)$, $\mathbf{v}_1(t)$, $\mathbf{v}_2(t)$ defined in (22) imply:

$$\begin{cases} \mathbf{i}_1(j) = & [\ -\dot{\mathbf{x}}^T(j) \quad i_{c1}(j) \quad \mathbf{i}_E^T(j)\ ]^T, \\ \mathbf{v}_1(j) = & [\ \nabla H^T(j) \quad v_{c1}(j) \quad \mathbf{v}_E^T(j)\ ]^T, \\ \mathbf{i}_2(j) = & [\ \mathbf{i}_{bR}^T(j) \quad \mathbf{i}_{tR}^T(j)\ ]^T, \\ \mathbf{v}_2(j) = & [\ \mathbf{v}_{bR}^T(j) \quad \mathbf{v}_{tR}^T(j)\ ]^T, \end{cases} \quad (31)$$

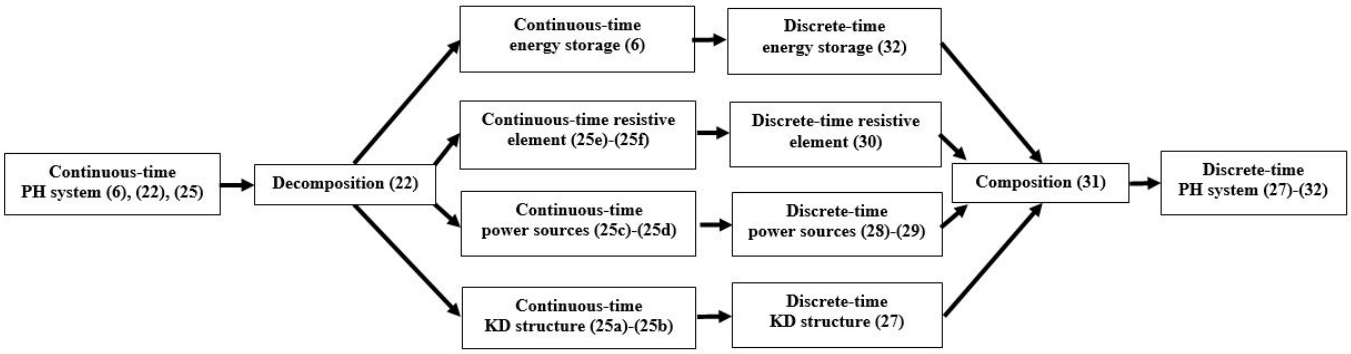

Figure 5: Time discretization process.

where $-\dot{\mathbf{x}}(j)$, $\nabla H(j) \in \mathbb{R}^2$ are the discrete vectors of the charge time derivative, $-\dot{\mathbf{x}}$, and of the Hamiltonian gradient vector, $\nabla H(\mathbf{x})$.

Now, we discuss about the discretization of the energy storage characterized by the flow and effort variables, $-\dot{\mathbf{x}}(j)$, $\nabla H(j)$. From (6) we note that the Hamiltonian, $H(\mathbf{x})$, is a quadratic function. Thus, we choose the following discrete-time scheme for the energy storage flow and effort variables, $-\dot{\mathbf{x}}(j)$, $\nabla H(j)$, as:

$$\begin{cases} -\dot{\mathbf{x}}(j) &= -\dfrac{\mathbf{x}(j)-\mathbf{x}(j-1)}{h}, \\ \nabla H(j) &= \mathbf{Q}_1 + \mathbf{Q}_2 \dfrac{\mathbf{x}(j)+\mathbf{x}(j-1)}{2}, \end{cases} \quad (32)$$

Remind that these variables represent the currents and the voltages of the energy storage elements in the battery. The discrete-time model of the microgrid defined by (27)-(32) preserves the energy balance equation as presented in Proposition 4.1 in [24].

Remark 4.1. *With other electricity storage units, the Hamiltonian $H(\mathbf{x})$ may have complex forms. However, there still exist different time-discretization methods guaranteeing the power-preserving and energy conservation properties of the microgrid [32, 33].*

Next, we formulate the optimization problem for the online scheduling of the battery operation with the twin goals of minimizing the price of the acquired electricity while in the same time respecting the constraints introduced earlier.

4.2. Scheduling formulation

As illustrated in Fig. 6 and also delineated in the discretized microgrid model (27) - (32), two control variables can be considered: the duty cycle $d(t)$ and the external grid current $i_e(t)$. Also, Fig. 6 illustrates the two-levels control scheme of the DC microgrid system. The lower level (corresponding to fast time scale) aims to keep the load voltage $v_l(t)$ constant, and the higher level (corresponding to slow time scale) deals with the optimal scheduling of the battery operation. In this work, we concentrate only on the latter problem, and the other is assumed to be achieved in the much faster time scale (e.g., [30, 31]) by using the duty cycle $d(t)$. Hence, at the lower level, we assume that the load voltage is forced to a desired value $v_{ref} \in \mathbb{R}$, that is, $v_l(t) = v_{ref}$, and at the higher level we consider that the only control variable is the external grid current, $i_e(t)$.

Hereinafter, we aim to minimize the electricity cost by an efficient scheduling of the power production and consumption with a storage unit serving as a filtering element. Due to the nature of the cost function (price dependent), the forthcoming approach can be classified as economic MPC.

By solving the following optimization problem over a finite prediction horizon N an open-loop optimal control sequence $\mathbf{i}_e(t) = \{i_e(0|t), \ldots, i_e(j|t), \ldots, i_e(N-1|t)\}$ is obtained at time instant t. It reacts to perturbations by incorporating feedback in the open-loop control problem, i.e., the first control action is applied as the system input:

$$i_e(0|t) = \underset{\mathbf{i}_e(t)}{\operatorname{argmin}} \sum_{j=1}^{N} \gamma.price(j|t) \cdot i_e(j|t) \cdot v_e(j|t), \quad (33)$$

subject to:

$$\begin{cases} \text{discrete-time dynamic (27)-(32),} \\ \text{constraints (3), (7), (9), (13),} \end{cases} \quad (34)$$

with $j = 1, \ldots, N$. Hence, by using the electricity price, $price(t)$ in the (33) we penalize buying and encourage selling[1].

[1]The selling and buying prices of the electricity are generally not the same. When taking into account different prices in the presented DC microgrid model leads to a Mixed-Integer Nonlinear Programming (MINLP) for the scheduling control formulation due to the dependence of the electricity price profile on the external grid current sign [21]. This implies the use of an integer variable indicating the external grid current sign in the cost function to enable switching between the buying or selling price. Some existing methods to deal with such MINLP problem may be found in the literature [34, 35].

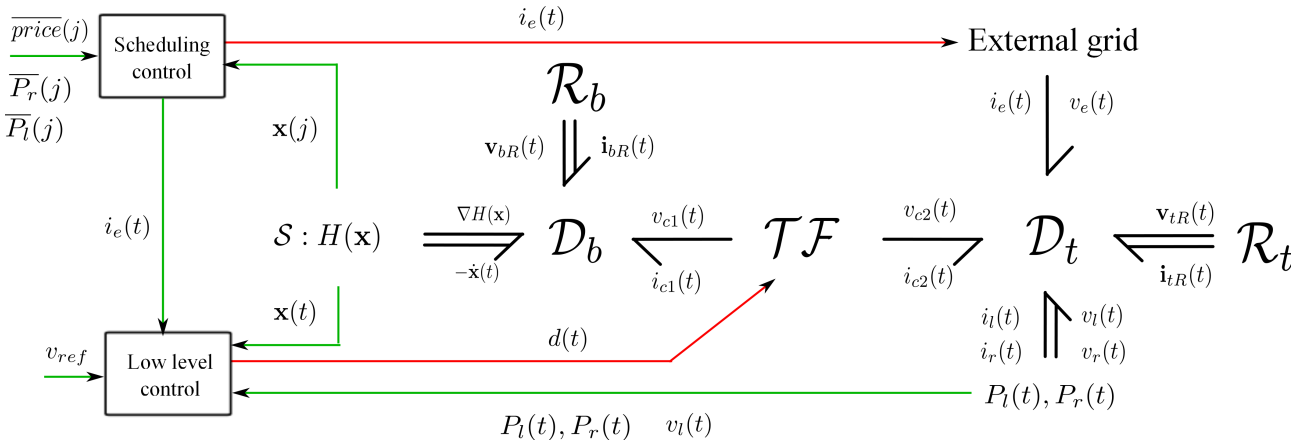

Figure 6: Scheduling control in the global control problem.

The profiles introduced in Section 3.4 appear as parameters here (e.g., the electricity price profile, $price(t)$, the load electrical power, $\bar{P}_l(t)$, and the renewable electrical power, $\bar{P}_r(t)$). Therefore, the cost (33) is variable due to the variation in the energy price, but otherwise is linear with respect to the input variable. We can see that the dynamics (25) and the constraints (3), (7), (9), (13) are overall nonlinear. Thus, the optimization problem is nonlinear both in cost and in constraints (as seen in (33)-(33)). The nonlinearity mainly comes from the transmission line resistor network and the high order battery model. They are important to evaluate the available stored electricity and the energy dissipation cost, thus, they can not be ignored by the MPC mechanism. Still, there are specialized solvers (like IPOPT, [36]) which can handle relatively large prediction horizons.

Note that the increase of the prediction horizon length N in (33) entails that the optimization problem minimizes the cost along the entire horizon. It may, however, be the case that the cost function is affected by uncertainties such that the cost values subsequent to the present values along the prediction horizon are less reliable. A solution is to vary the weight $\gamma \in (0, 1)$ from (33) associated to each cost value over the prediction horizon (i.e., varying γ we may assign less importance to the cost values which are further in the future [37]).

We can see that, in the slow time scale, the power balance implies a zero sum of the components power which is guaranteed by the power-preserving discretization of the system dynamics as presented in Section 4.1. However, the power balance problem is more challenging when considering the components constraints. Therefore, the microgrid power balance is satisfied if the constrained optimization problem (33)-(34) is feasible at all time. In other words, the power balance equation is one of the constraints of the MPC problem. Hence, whenever the MCP is feasible (i.e., returns an optimal solution), it means that the constraint was verified, hence ensuring the power balance within the grid. Note that correctly design MPC can be guaranteed to be recursive feasible and that practically, in our simulations, we did not encountered infeasibility or numerical issues.

This work employs a centralized MPC which is generally not robust to failure (renewable generator fault, transmission lines faults and the like). Therefore, distributed MPC [38] is a promising approach for complex microgrids. However, most of the applications for such systems are for tracking objective with convex cost functions. For nonlinear costs (e.g., electricity cost), the global optimality is more difficult to ensure.

5. Simulation results

This section presents simulation and comparison results under different scenarios for the operation and control of the DC microgrid elevator system illustrated in Fig. 1 and equivalently represented by the electrical DC circuit in Fig. 2.

The forthcoming simulations use the reference profiles described in Section 4 and the battery parameters presented in (6)-(9) with the numerical data given by the industrial partner Sodimas. They are illustrated in Fig. 4 and Table 2.

We first provide results for nominal and the uncertainty-affected electrical power of load and renewable unit. Next, comparisons with other microgrid models and approaches are considered. For further use, we define SoC (States of Charge) criteria which characterize the battery state $\mathbf{x} \in \mathbb{R}^2$, given in (6):

$$SoC_1 = \frac{x_1}{x_{1,max}}, \quad SoC_2 = \frac{x_2}{x_{2,max}}, \tag{35a}$$

$$SoC = \frac{x_1 + x_2}{x_{1,max} + x_{2,max}}. \tag{35b}$$

where $x_{1,max}$, $x_{2,max}$ and q_{max} are the maximal charges defined in (7) - (8).

Remark 5.1. *We are aware that the battery's capacity may be affected by multiple variables: temperature, age, even discharge current. Thus, the SoC may in fact depend nonlinearly on the current, but we consider the linear relation given in equation (26) and (35) a fair approximation [26].*

Table 2: Numerical data for the microgrid components

Name	Notation	Value
Battery parameters	$\mathbf{Q}_1$ $[V]$	$[\ 13 \quad 13\ ]^T$
	$\mathbf{Q}_2$ $[V/C]$	diag $\{0.3036, 0.2024\}$
Battery constraints	$\mathbf{x}_{max}$ $[Ah]$	$[\ 73.2 \quad 109.8\ ]^T$
	$i_{b,min}$ $[A]$	-20
	$i_{b,max}$ $[A]$	20
Grid constraints	$i_{e,min}$ $[A]$	-8
	$i_{e,max}$ $[A]$	8
Bus voltage reference	v_{ref} $[V]$	380
Resistors	R_1 $[\Omega]$	0.012
	R_2 $[\Omega]$	0.015
	R_{bl} $[\Omega]$	0.31
	R_{be} $[\Omega]$	0.29
	R_{er} $[\Omega]$	0.23
	R_{rl} $[\Omega]$	0.19
Scheduling time step	h $[hour]$	0.5
Prediction horizon	N	48
Weighting parameter	$\gamma \in (0, 1)$	0.5

The numerical optimization problem is solved by using Yalmip ([39]) and IPOPT ([40]) in Matlab 2013a. The constrained closed-loop dynamics implementation are done by using the *fsolve* function in Matlab 2013a with a fixed sampled time of 36 seconds over a horizon of 24 hours. Note that this sampling time corresponds to the discretization of the continuous nonlinear dynamics. The update of the power profiles happens every 30 minutes, which is described by setting the value of the scheduling time step, h, at 0.5 hours as detailed in Table 2.

Considering the numerical data in Table 2 and the reference profiles in Fig 4 some remarks are in order:

Remark 5.2. *For this particular DC microgrid system the maximum supplied power (the sum of the PV and the battery) is always less than the load power*[2]*. This means that with the numerical data we have at our disposal the microgrid cannot operate in islanded mode, i.e., disconnected from the external grid. Also, the maximum amount of power provided by the external grid is greater than the load power. These statements are summarized by the following expressions:*

$$v_{b,max} i_{b,max} + P_r(t) < P_l(t) < v_{ref} i_{e,max},\ \forall t, \qquad (36)$$

where $v_{b,max}$, the maximum voltage of the battery (see Fig. 2), satisfies:

$$v_{b,max} = [1\ 0]\,(\mathbf{Q}_1 + \mathbf{Q}_2 \mathbf{x}_{max}) + R_2 i_{b,max},$$

with the battery resistor R_2 given in Table 2.

[2]This provides further justification for the use of the PV model (5).

Remark 5.3. *In the grid-connected operation of the DC microgrid, the voltages of the DC bus and of the battery are always positive, i.e., $v_{c2}(t) > 0$, $v_{c1}(t) > 0$. Thus, the duty cycle is positive according to* (12)*.*

Therefore, in this particular case, the constraints of the external grid current (3) and of the duty cycle (13) can be ignored.

5.1. Nominal scenario

Fig. 9 illustrates in the nominal scenario the battery charges $\mathbf{x}(t)$ along the simulation horizon (i.e., 24h). From 7 to 9 o'clock, the first charge (SoC_1) attains the maximal limit but the second (SoC_2) and total one (SoC) do not. It means that the battery can still be charged but with a smaller current. Also, since the battery charges respect their constraints, we can conclude that the load power demand is always satisfied.

Fig. 7 describes the actual electrical power charged/discharged by the DC components. Note that their positive signs indicate that the power is supplied to the microgrid. Also, it can be observed that when the electricity price is cheap, the battery is charged. Conversely, it is discharged during the high load and expensive electricity price intervals. Furthermore, to minimize the cost, the battery is discharged completely to half its maximum capacity at the end of the day in preparation for the next day.

Increasing the battery capacity has a diminishing effect on the overall cost reduction. We tested this assumption in simulation as illustrated in Fig. 8. Above a capacity of 13 times the initial capacity value q_{max} as described by (8) there is no discernible improvement. This is justified by the fact that there is enough capacity to reduce at minimum the external grid demand. In fact this may change with the length of the prediction horizon or with a varying electricity price (where it makes sense for the battery to arbitrate the fluctuations).

Furthermore, increasing the solar panel power has a diminishing effect on the overall cost reduction. We tested this assumption in simulation as illustrated in Fig. 10. Above an amount of photovoltaic power of 3 times the initial profile $P_r(t)$ described in Fig. 4, the electricity cost is negative. This is justified by the fact that the solar power is enough to satisfy the load demand and to sell the electricity to the external grid. However, even if this situation happens, we can not ensure the isolated mode of the microgrid.

5.2. Uncertainty-affected scenario

In order to investigate how the economic MPC approach reacts to uncertainties we consider in the following 6 uncertainty-affected scenarios:

- Scenario 1: perturbation-affected power profiles of the load and renewable source, $P_l(t)$ and $P_r(t)$,

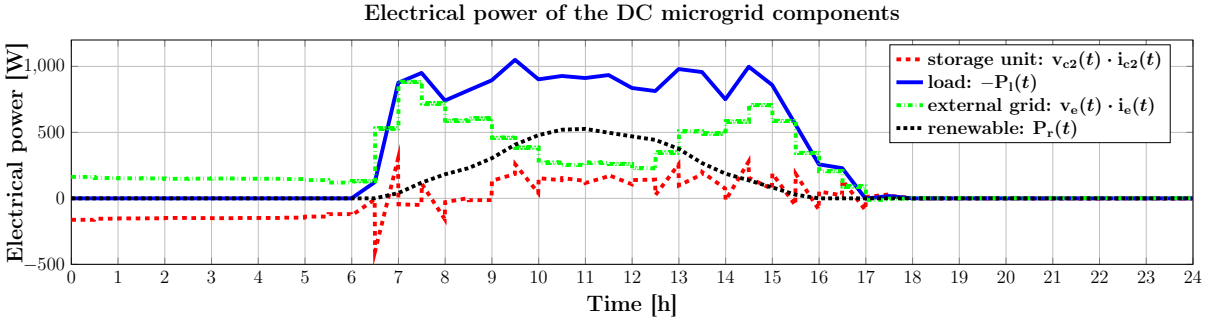

Figure 7: Nominal scenario: actual electrical power charge/discharge by the DC components.

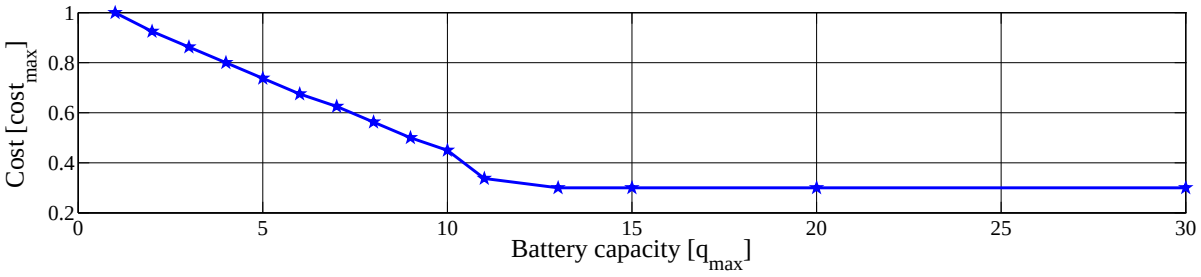

Figure 8: Nominal scenario: cost and battery capacity relation.

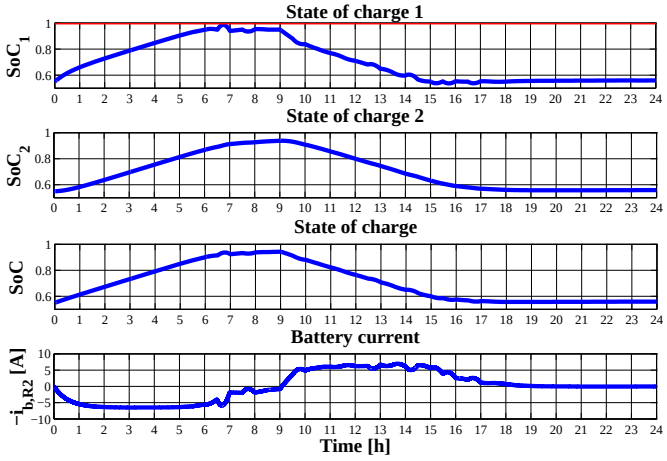

Figure 9: Nominal scenario: battery state of charges (SoC_1, SoC_2, SoC as defined in (35)) and discharge current.

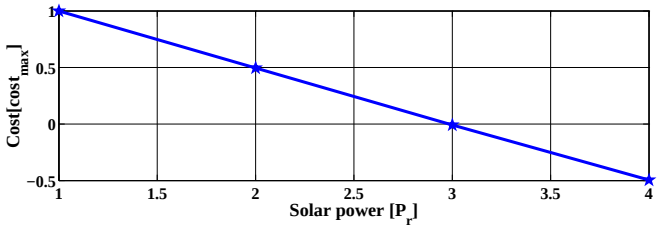

Figure 10: Nominal scenario: cost and solar panel power relation.

- Scenario 2: proportional uncertainties-affected power profiles of the load and renewable source, $P_l(t)$ and $P_r(t)$,
- Scenario 3: proportional uncertainties of the battery voltages, $\mathbf{Q}_1 \in \mathbb{R}^2$,
- Scenario 4: proportional uncertainties of the battery capacitors, $\mathbf{Q}_2 \in \mathbb{R}^{2\times 2}$,
- Scenario 5: proportional uncertainties of the resistors.
- Scenario 6: intermittent power profile of the renewable source.

Scenario 1: The perturbation is assumed to be bounded in a symmetrical tube. More precisely, the electrical power of load and renewable source are within some uncertainty ranges:

$$P_l(t) \in \overline{P_l}(t)\,[1-\epsilon_{lmin}, 1+\epsilon_{lmax}]\,, \tag{37a}$$

$$P_r(t) \in \overline{P_r}(t)\,[1-\epsilon_{rmin}, 1+\epsilon_{rmax}]\,, \tag{37b}$$

where $\epsilon_{(.)}$ are positive numbers taken here as $\epsilon_{lmin} = \epsilon_{lmax}$, $\epsilon_{rmin} = \epsilon_{rmax}$ with the values set to 0.2.

The battery state of charge and components electrical power are presented in Figs. 12 and 11. Fig. 12 illustrates the battery state of charge (for the situations considered in (37)) with bounded uncertainty affecting the electrical power load and renewable. We can observe that the battery charge respects the imposed constraints and the load

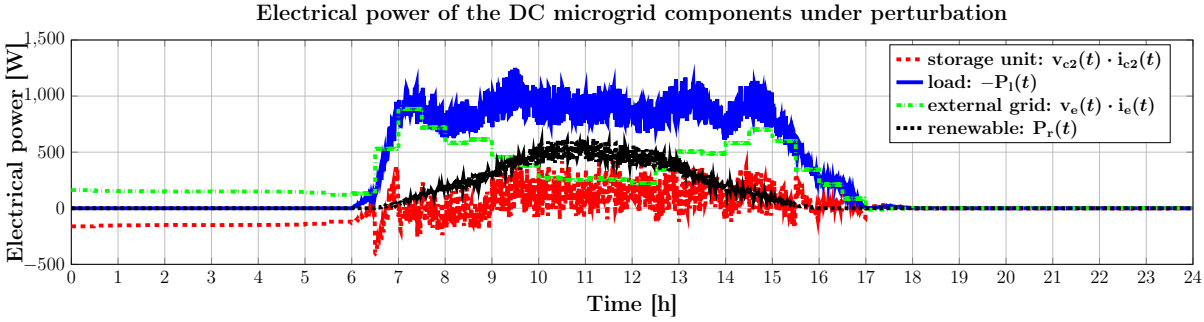

(a)

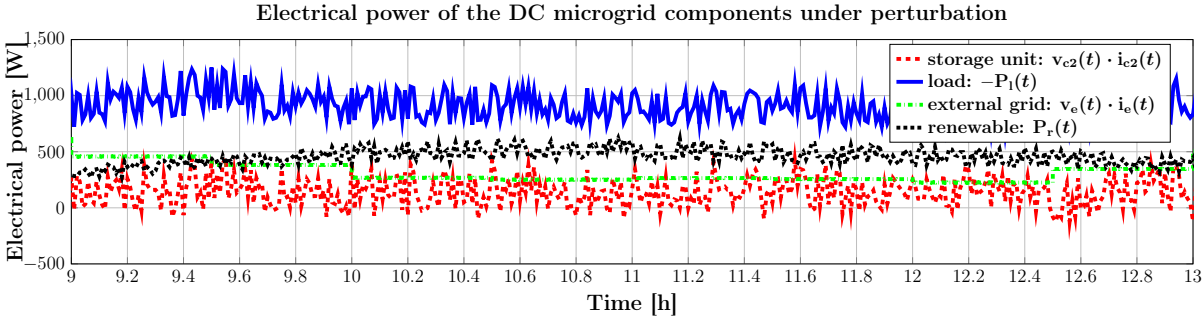

(b)

Figure 11: (a) Scenario 1: actual electrical power charged/discharged by the DC components under perturbation scenario. (b) Zoom for the subfigure (a).

power demand is always satisfied. Note that this result is not significantly different from the nominal case in Fig. 9. This is due to the fact that we consider a uniformly distribute noise as specified by (37), and thus, the variations cancel each other.

Furthermore, Fig. 11 describes the components, actual provided electrical power under the uncertainty-affected scenario. Since the current (and power) of the external grid is fixed, most of the fluctuation of the microgrid electrical power is absorbed by the battery.

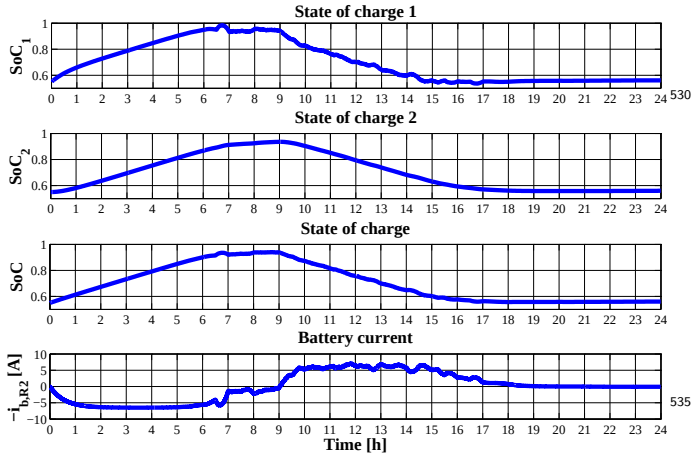

Figure 12: Scenario 1: battery state of charges (SoC_1, SoC_2,SoC as defined in (35)) and discharge current (perturbation scenario).

Scenario 2: The actual renewable power profile is proportional to the reference profile:

$$P_r(t) = \alpha \overline{P_r}(t), \ \forall t, \tag{38}$$

where α is positive with its value chosen in the set $\{0.8, 1, 1.2, 1.4\}$. The battery charge profiles with these values of α are illustrated in Fig. 13. In the morning (from 0h to 8h), since there is no renewable power, the proportional uncertainty has no effect on the battery charge policy. During the sunny period, since the power supplied by the external grid is fixed during a prediction time step (i.e., 30 minutes), the difference between the amounts of uncertainty-affected and predicted power will be supported by the battery.

Scenario 3: The battery voltage parameter, $\mathbf{Q}_1$, in (6) is proportional to the reference value, $\overline{\mathbf{Q}_1}$:

$$\mathbf{Q}_1 = \beta_1 \overline{\mathbf{Q}_1}, \tag{39}$$

where β_1 is positive with its value chosen in the set $\{0.8, 1, 1.2\}$. SoC_1 values of the battery, as defined in (35a), are illustrated in Fig. 14 for the β_1 parameters. When the power balance of the microgrid is guaranteed, the charged power of the battery is equal to the supplied power of the other components (external grid, renewable source, load). With the same charged power, when β_1 increases, the battery voltage increases, and thus, the battery current decreases. Therefore, the battery is charged

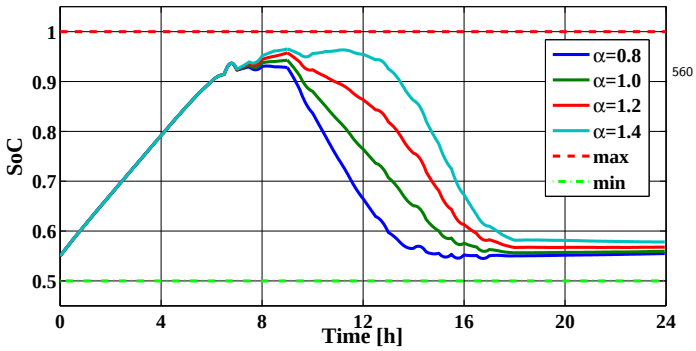

Figure 13: Scenario 2: battery charge defined in (35b) with proportional uncertainties of the renewable power as in (38).

slower as shown in Fig. 14 between 0h and 8h. The contrary situation happens when the battery is discharged between 8h and 17h. Moreover, if the real battery voltage parameter is too small w.r.t the reference value, the battery charge passes the limits which is not predicted in the scheduling controller.

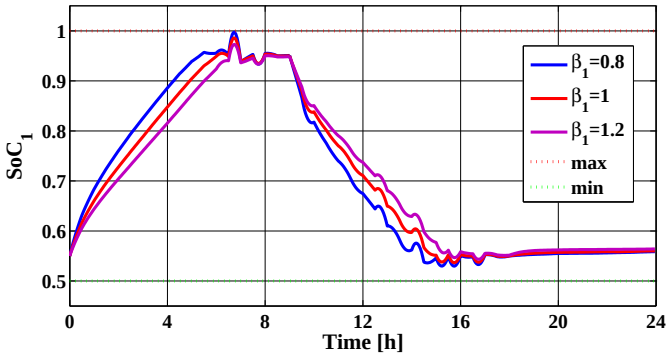

Figure 14: Scenario 3: SoC_1 of the battery, as defined in (35a), with proportional uncertainties of the battery voltage parameter as in (39).

Scenario 4: The uncertainty of the battery capacity parameter, $\mathbf{Q}_2$, in (6) is proportional to the reference value, $\overline{\mathbf{Q}_2}$:

$$\mathbf{Q}_2 = \frac{1}{\beta_2}\overline{\mathbf{Q}_2}, \tag{40}$$

where β_2 is positive with its value chosen in the set $\{0.01, 0.1, 1, 1.5\}$. Note that $\mathbf{Q}_2^{-1}$ characterizes the capacities of the capacitors in the battery model (see figure 2). Thus, from the electrical meaning of the ratio, we use here $1/\beta_2$ instead of β_2. SoC_1 of the battery, as defined in (35a), is illustrated in Fig. 15 for the various parameters β_2. Note that $\beta_2 > 1$ implies that the actual battery capacitors (see also Fig. 2) are greater than the reference values. We see that with the same charge, increasing the capacities of the battery capacitors decreases the battery voltage. This increases the battery charge/discharge current. Therefore, the battery state of charge, SoC, increases when increasing β_2 in the charge case, and decreases in the discharge case. Consequently, if the real battery capacity parameter is too high w.r.t the reference value, the battery charges, $x_1(t)$, $x_2(t)$, may trespass the limits.

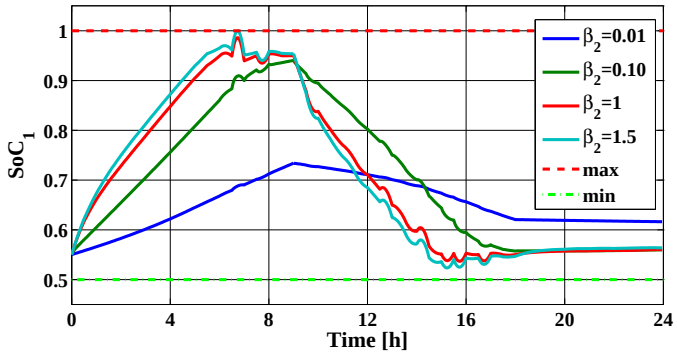

Figure 15: Scenario 4: Soc_1 of the battery, as defined in (35a), with proportional uncertainties of the battery capacity parameter as in (40).

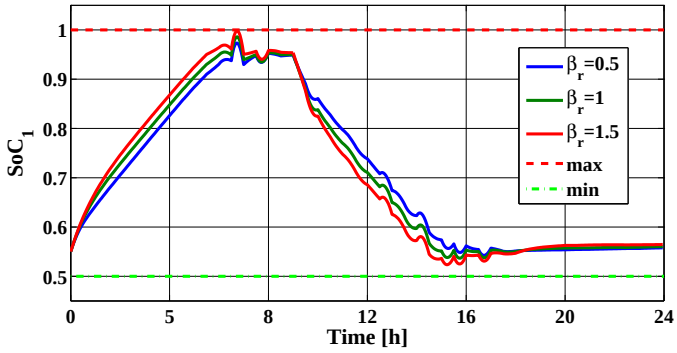

Figure 16: Scenario 5: SoC_1 of the battery, as defined in (35a), with proportional uncertainties of the resistors as in (41).

Scenario 5: The resistor matrices $\mathbf{R}_b$ and $\mathbf{R}_t$ in (10) and (14) are proportional to the reference values, $\overline{\mathbf{R}_b}$ and $\overline{\mathbf{R}_t}$:

$$\mathbf{R}_b = \beta_r\overline{\mathbf{R}_b},\ \mathbf{R}_t = \beta_r\overline{\mathbf{R}_b}, \tag{41}$$

where β_r is positive with its value chosen in the set $\{0.5, 1, 1.5\}$. SoC_1 of the battery, as defined in (35a), is illustrated in Fig. 16, for the various parameters β_r. $\beta_r > 1$ implies that the resistor R_1 between the two internal charges of the battery is greater than the reference value. Therefore, the current through R_1 is smaller than this current in the nominal case. Thus, the charge from the first battery charge $x_1(t)$ to the second charge $x_2(t)$ flows more slowly, and $x_1(t)$ increases faster in the charge case.

Scenario 6: The solar power is cut-out for a duration of 30 minutes at 8 o'clock and 10 o'clock. The battery state of

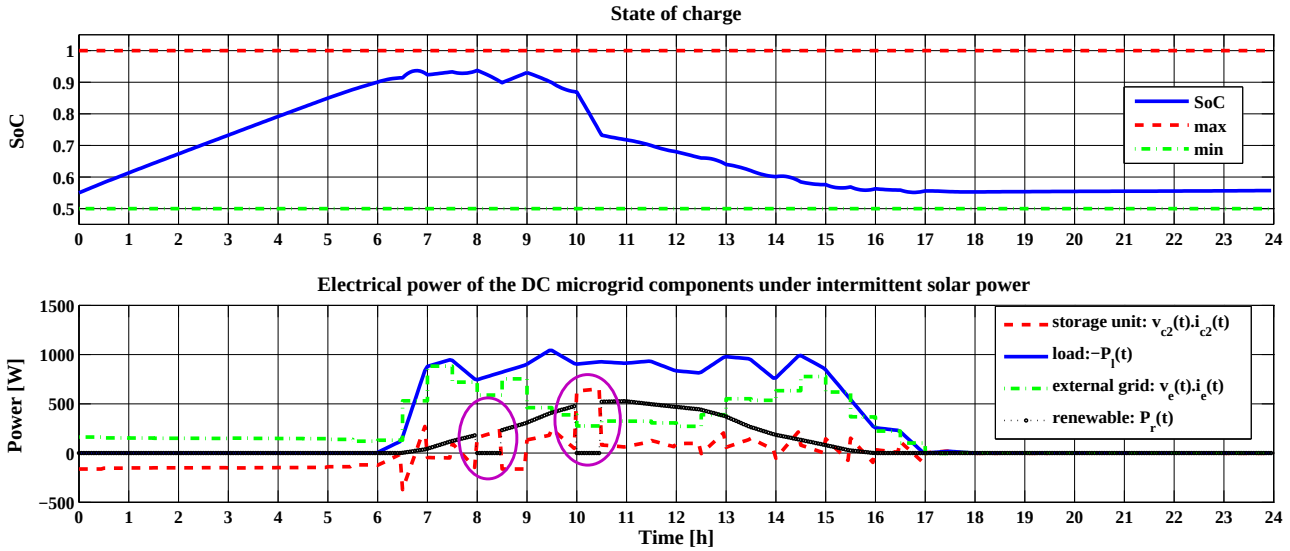

Figure 17: Scenario 6: battery SoC in (35b) and electrical power of the DC microgrid components under the intermittent renewable power.

charge and the electrical power of the DC microgrid components are illustrated in Fig. 17. In this scenario, since the scheduling control does not predict this intermittent power period, the battery will support the missing power from the renewable source. Then, the battery recharges from the external grid after these periods. The electricity cost of this scenario is illustrated in Table 3. We observe that it is higher than the electricity cost of the nominal scenario since more electricity must be purchased from the external grid when the renewable source is cut-out.

Table 3: Electricity cost [Euros] in two scenarios: nominal and intermittent photovoltaic power.

Scenario	Cost [Euros]
Nominal	0.7989
Intermittent photovoltaic power	0.8480

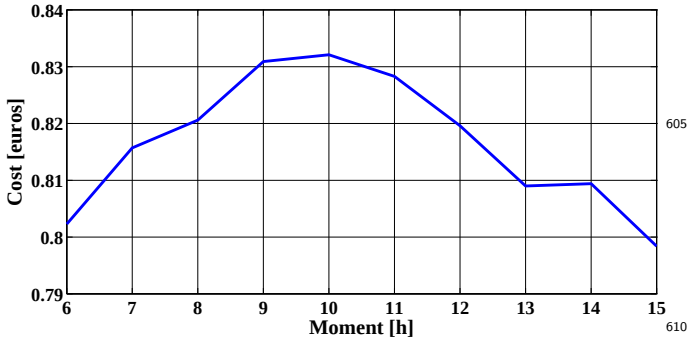

Figure 18: Scenario 6: electricity cost with different time moments of the cut-out photovoltaic power.

In another scenario, the renewable power is cut-out one time a day during 24 minutes at different time moments. Fig. 18 illustrates the electricity cost of the DC microgrid during a day with these cut-out power moments. We see that the cost is maximal when the renewable power is cut-out at 10 o'clock. This is due to the fact that the solar panel generates the maximal power at this moment in the expensive electricity period. When it is cut-out, the battery supports this maximal missing power and is maximally recharged from the external grid later. Thus, the electricity cost for the day when the photovoltaic power is cut-out at 10 o'clock is the most expensive with respect to other cut-out time moments.

The above simulation scenarios validate the robustness of the proposed control approach with different types of uncertainty. Next, the microgrid model used in this control approach is compared with other models.

6. Comparison with other models and control strategies

Now, we apply the presented economic MPC using two others models and a rule-based approach for the DC microgrid. Then, we compare the economic efficiencies of these methods with the control laws designed in the previous sections.

6.1. Reduced model with explicit Euler discretization scheme

The reduced model considered here is similar to the microgrid models in [8, 28]. In these works, the authors consider constant battery dissipation and additionally take into account the battery self-discharging phenomenon. However, these issues do not lead to important differences of the battery behavior.

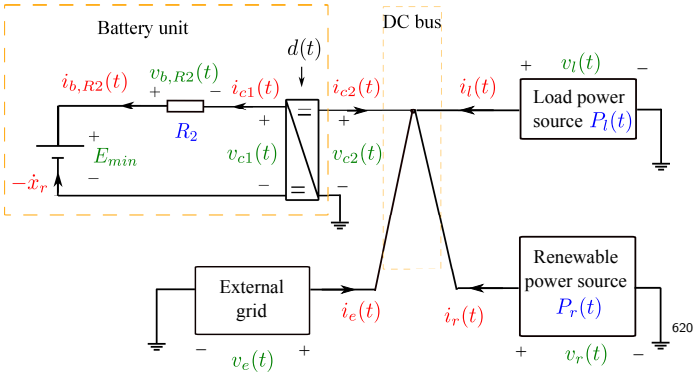

Figure 19: Electrical circuit of the DC microgrid reduced model.

This model can be obtained from the model presented in Section 3 by reducing the resistors of the battery, R_1, and of the transmission lines, $\mathbf{R}_t$ in (14):

$$R_1 \approx 0,\ \mathbf{R}_t \approx \mathbf{0}, \tag{42}$$

and by assuming that the battery charge does not modify the battery voltage, that is:

$$\mathbf{Q}_2 q_{max} \mathbf{1}_2 << \mathbf{Q}_1, \tag{43}$$

where $\mathbf{Q}_1$, $\mathbf{Q}_2$ are the weight matrices defined in (6), and q_{max} is the battery capacity defined in (7). Consequently, the battery is modeled as a series electrical circuit of a voltage source E_{min} and a resistor R_2 as in Fig. 19. There is only one state variable $x_r(t) = x_1(t) + x_2(t)$ which leads to the following energy function of the battery:

$$H_r(x_r) = E_{min} x_r(t). \tag{44}$$

Considering the assumptions (42)-(44), we obtain the following continuous-time dynamics of the DC microgrid.

Proposition 6.1. *The reduced microgrid model associated with the low level control (see Fig. 6) admits the following dynamics:*

$$\dot{x}_r(t) = \frac{2P_b(t)}{E_{min} + \sqrt{E_{min}^2 + 4R_2 P_b(t)}}, \tag{45}$$

where $P_b(t) \in \mathbb{R}$ is the battery charged power which is equal to the sum of the power from the external grid, the renewable source and the load:

$$P_b(t) = v_{ref} i_e(t) + P_r(t) - P_l(t). \tag{46}$$

The energy charging efficiency is, then, derived as:

$$\eta(P_b) = \frac{2}{1 + \sqrt{1 + \frac{4R_2}{E_{min}^2} P_b(t)}}. \tag{47}$$

Proof. See Appendix A for details. □

Then, the discrete-time microgrid dynamics is obtained using the explicit Euler scheme:

$$x_r(j+1) = x_r(j) + \frac{2hP_b(j)}{E_{min} + \sqrt{E_{min}^2 + 4R_2 P_b(j)}}, \tag{48}$$

where h is the time step, and

$$P_b(j) = v_{ref} i_e(j) + P_r(j) - P_l(j). \tag{49}$$

We can observe that this microgrid model (48)-(49) simplifies the complexity of the optimization problem given in (33)-(34). However, it ignores the internal resistance between different sub-storage parts of the battery. Thus, the directly available battery charge in the control prediction is higher than the actual one. Another limit of this reduced battery model relates to the description of the energy efficiency. This efficiency is obviously smaller than 1 due to the voltage drop and the electricity loss [41]. Moreover, both of these elements depend on different factors such as the battery State-of-Charge (SoC) and the charging/discharging rate. From Proposition 6.1, we note that the simplified model takes into account the voltage drop with the dependence on the charging/discharging rate. However, the influence of the SoC level is ignored, which may lead to an important overestimation of the energy amount in the battery, and thus, lead to less energy supplied to the load.

6.2. Detailed model with the explicit Euler discretization scheme

To obtain this model, we discretize the continuous-time model of the DC microgrid in Section 3 using the explicit Euler scheme (details of the explicit Euler method can be found in [42]). In this scheme, the discretization of the microgrid network, the power sources, the resistors defined in (27)-(31) are similar, but the discretization of the energy storage element is different from (32), that is:

$$\begin{cases} -\dot{\mathbf{x}}(j) &= -\dfrac{\mathbf{x}(j) - \mathbf{x}(j-1)}{h}, \\ \nabla H(j) &= \mathbf{Q}_1 + \mathbf{Q}_2 \mathbf{x}(j-1). \end{cases} \tag{50}$$

Note that this Euler discretization scheme does not preserve the energy balance (see also (**??**)) since:

$$H(\mathbf{x}(j)) - H(\mathbf{x}(j-1)) > \int_{(j-1)h}^{jh} [P_l(t) + P_r(t)]dt + \\ + i_e(j) v_e(j) h - \mathbf{i}_{bR}^T(j) \mathbf{R}_b \mathbf{i}_{bR}(j) h - \mathbf{i}_{tR}^T(j) \mathbf{R}_t \mathbf{i}_{tR}(j) h.$$

6.3. Rule-based control approach

The rule-based control formulates explicit control laws for the microgrid based on the current battery State of Charge, SoC, required power of the load and the supplied power of the renewable source [1, 29]. Let $i_d(t)$ be the necessary values of the battery charge current to guarantee the power balance of the microgrid without the external grid,

i.e., $i_e(t) = 0$, $SoC(t)$ be the battery state of charge given as in (35b), $i_{b,min}, i_{b,max}$ be the minimum and maximum battery charge current given in (9). Since for each external grid current, $i_e(t)$, there exists only one battery charge current, $i_{c1}(t)$, such that the microgrid power is balanced, we can alternatively choose $i_{c1}(t)$ as the control variable. Based on [1, 29], the control variable $i_{c1}(t)$ is given in Table 4. Thus, we note that the rule-based control does not take into account the prediction of the renewable power, the load power and the electricity price.

Table 4: Rule-based control laws, $i_{c1}(t)$.

$i_d(t) \backslash SoC(t)$	$0.5q_{max}$	$(0.5q_{max}, q_{max})$	q_{max}
$(-\infty, i_{b,min})$	0	$i_{b,min}$	$i_{b,min}$
$(i_{b,min}, 0)$	0	$i_d(t)$	$i_d(t)$
$(0, i_{b,max})$	$i_d(t)$	$i_d(t)$	0
$(i_{b,max}, +\infty)$	$i_{b,max}$	$i_{b,max}$	0

6.4. Simulation results

In the forthcoming simulation scenarios, we consider the four following controllers:

- Controller 1: solves the optimization problem provided in (33)-(34) using the detailed model with the energy-preserving discretization scheme given in (27)-(32),
- Controller 2: solves the optimization problem provided in (33)-(34) using the detailed model with the explicit Euler discretization scheme (27)-(31) and (50),
- Controller 3: solves the optimization problem provided in (33)-(34) using the reduced model with the explicit Euler discretization scheme (48)-(49),
- Controller 4: implements the rule-based control approach from Table 4.

The simulations are implemented with different battery current limits, that is, $i_{b,max} = -i_{b,min} \in \{5, 10, 20\}$ $[A]$. The electricity costs corresponding to these scenarios are illustrated in Table 5.

Table 5: Electricity cost [Euros] with different battery current limits and different control formulations.

$i_{b,max}$ [A]\Controller	1	2	3	4
5	0.8134	0.8246	0.8582	0.8653
10	0.7992	0.7992	0.8022	0.9126
20	0.7989	0.7987	0.7962	0.9479

When the maximum battery current is 20A, the electricity cost of Controller 1, 2, and 3 are nearly the same. This is due to the fact that the battery is charged and discharged during the same period with the same charge (see also Fig. 20). Controller 4 leads to a higher cost since it discharges when the electricity price is cheap. Thus, during the expensive electricity price period (from 9 to 18 o'clock), it is empty, and the external grid supplies the power to the load (see also Fig. 20). Moreover, the battery is recharged at the end of day with the electricity purchased from the external grid.

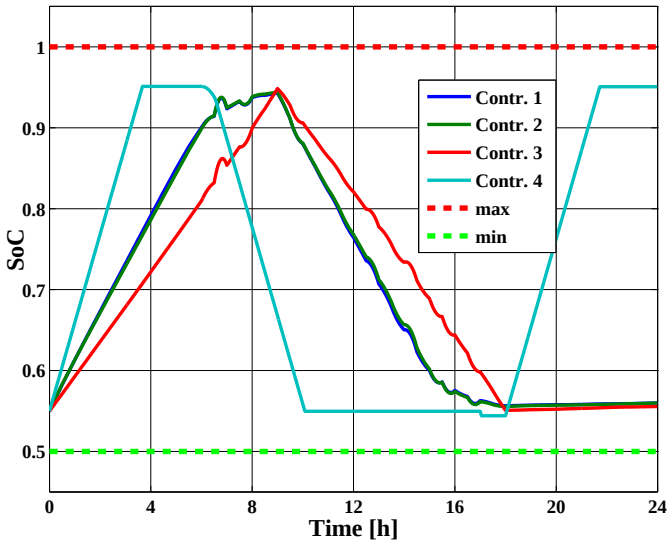

Figure 20: Battery charges corresponding to different controllers with $i_{b,max} = 20A$.

When the maximum battery current is 5A, with these four controllers, the battery is not fully charged during the day (see also Fig. 21). This is due to the fact that it has to be discharged when the electricity price is expensive (Controllers 1, 2 and 3) or when there is a load demand (Controller 4). Not in the least, before it is discharged (9 o'clock for Controllers 1, 2 and 3, 6 o'clock for Controller 4), the maximum battery currents are too small to fully charge the battery.

Furthermore, in these scenarios (corresponding to $i_{b,max} = 5\ A$), the electricity cost of Controller 1 is smaller than the costs of Controllers 2, 3 and 4. This is due to two following reasons. First, the battery discharge of Controllers 2, 3 and 4 is smaller than the discharge of Controller 1 during the expensive electricity price period (from 9 to 18 o'clock). Thus, more electricity is purchased from the external grid to satisfy the load demand. Second, with Controllers 2, 3 and 4, the battery charges at the end of the day.

7. Conclusion

This paper introduced an efficient power scheduling for a DC microgrid using a combination of economic Model Predictive Control and Port-Hamiltonian formulations. Firstly, a detailed model of the DC microgrid system was presented. Its dynamics were described using Port-Hamiltonian formulations on graphs to preserve the energy and power conservation properties and to capture the microgrid topology. Next, a nonlinear constrained

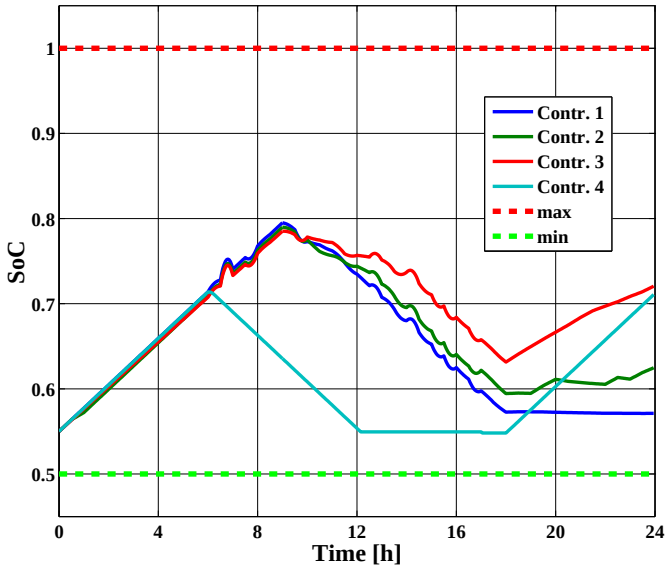

Figure 21: Battery charges corresponding to different controllers with $i_{b,max} = 5$ A.

optimization problem was formulated for power scheduling taking into account the microgrid dynamics, operating constraints and predictions of the load demand, of the renewable power and of the electricity price. The proposed control approach was validated through simulation results which investigated the control robustness and illustrated the economic efficiency of the controller with respect to other standard methods.

As future work, we envision several directions of improvement for the constrained optimization-based control scheme: i) stability by considering the properties and specific form of the Port Hamiltonian formulations; ii) robustness by taking explicitly in consideration the disturbances; iii) low level control for the converter and the DC bus using tracking Model Predictive Control.

Acknowledgement

This work has been partially funded by the European Artemis ARROWHEAD project under grant agreement number 332987.

Appendix A. Proof of Proposition 6.1

This section introduces the proof for Proposition 6.1. Using the Kirchhoff's laws for the electrical circuit in Fig . 19 we obtain:

$$\begin{cases} i_{c2}(t) + i_l(t) + i_e(t) + i_r(t) &= 0, \\ v_{c2}(t) = v_l(t) = v_e(t) &= v_r(t), \\ \dot{x}_r(t) = i_{b,R2}(t) &= i_{c1}(t), \\ E_{min} - v_{b,R2}(t) - v_{c1}(t) &= 0. \end{cases} \tag{A.1}$$

Thanks to the low control level, the DC bus voltage is equal to the reference value v_{ref}. Let the power of the external grid, battery unit, renewable source and load be denoted by:

$$\begin{cases} P_e(t) = & i_e(t)v_e(t), \\ P_b(t) = & -i_{c2}(t)v_{c2}(t), \\ P_l(t) = & -i_l(t)v_l(t), \\ P_r(t) = & i_r(t)v_r(t). \end{cases} \tag{A.2}$$

From (12) and (A.1)-(A.2), we derive the following equation of the duty cycle:

$$v_{ref}^2 d(t)^2 - E_{min} v_{ref} d(t) - R_2 P_b(t) = 0. \tag{A.3}$$

There are two roots for the previous equation:

$$d(t) = \frac{E_{min} \pm \sqrt{E_{min}^2 + 4R_2 P_b(t)}}{2v_{ref}}. \tag{A.4}$$

In the case $P_b(t) > 0$, since the duty cycle $d(t)$ is positive,

$$d(t) = \frac{E_{min} + \sqrt{E_{min}^2 + 4R_2 P_b(t)}}{2v_{ref}}. \tag{A.5}$$

In the case $P_b(t) < 0$, two roots of (A.4) are positive, but with (A.5) the dissipated energy is smaller. Using this formulation of the duty cycle with (12) and (A.1)-(A.2), we obtain the microgrid dynamics (45)-(46), and the energy efficiency (47).

References

[1] C. Yin, H. Wu, F. Locment, M. Sechilariu, Energy management of DC microgrid based on photovoltaic combined with diesel generator and supercapacitor, Energy Conversion and Management 132 (2017) 14–27.

[2] J. Barreiro-Gomez, C. Ocampo-Martinez, F. D. Bianchi, N. Quijano, Data-driven decentralized algorithm for wind farm control with population-games assistance, Energies 12 (6) (2019) 1–14.

[3] S. Siniscalchi-Minna, F. Bianchi, M. D. Prada-Gil, C. Ocampo-Martinez, A wind farm control strategy for power reserve maximization, Renewable Energy 131 (2019) 37–44.

[4] A. Conejo, R. Sioshansi, Rethinking restructured electricity market design: Lessons learned and future needs, International Journal of Electrical Power & Energy Systems 98 (2018) 520–530.

[5] A. Iovine, T. Rigaut, G. Damm, E. D. Santis, M. D. D. Benedetto, Power management for a dc microgrid integrating renewables and storages, Control Engineering Practice 85 (2019) 59 – 79.

[6] Peng Kou, D. Liang, L. Gao, Distributed Coordination of Multiple PMSGs in an Islanded DC Microgrid for Load Sharing, IEEE Transactions on Energy Conversion 32 (2) (2017) 471 – 485.

[7] P. Kou, D. Liang, J. Wang, L. Gao, Stable and optimal load sharing of multiple PMSGs in an islanded DC microgrid, IEEE Transactions on Energy Conversion 33 (1) (2018) 260 – 271.

[8] A. Parisio, E. Rikos, L. Glielmo, Stochastic model predictive control for economic/environmental operation management of microgrids: an experimental case study, Journal of Process Control 43 (2016) 24–37.

[9] C. Touretzky, M. Baldea, A hierarchical scheduling and control strategy for thermal energystorage systems, Energy and Buildings 110 (8) (2016) 94–107.

[10] E. Trélat, Optimal control and applications to aerospace: Some results and challenges, Journal of Optimization Theory and Applications 154 (2012) 713–758.

[11] S. Siad, A. Malkawi, G. Damm, L. Lopes, L. Dol, Nonlinear control of a DC MicroGrid for the integration of distributed generation based on different time scales, International Journal of Electrical Power & Energy Systems 111 (2019) 93–100.

[12] M. Alamir, M. Rahmani, D. Gualino, Constrained control framework for a stand-alone hybrid, Applied Energy 118 (2014) 192–206.

[13] J. Lagorse, D. Paire, A. Miraoui, A multi-agent system for energy management of distributed power sources, Renewable Energy 35 (1) (2010) 174–182.

[14] M. Sechilariu, B. Wang, F. Locment, Supervision control for optimal energy cost management in DC microgrid: Design and simulation, International Journal of Electrical Power & Energy Systems 58 (2014) 140–149.

[15] D. Lifshitz, G. Weiss, Optimal control of a capacitor-type energy storage system, IEEE Transactions on Automatic Control 60 (1) (2014) 216–220.

[16] L. T. dos Santos, M. Sechilariu, F. Locment, Optimized load shedding approach for grid-connected DC microgrid systems under realistic constraints, Buildings 6 (4) (2016) 50.

[17] J. M. Maciejowski, Predictive control with constraints, Prentice Hall, 2002.

[18] J. Rawlings, D. Mayne, Model Predictive Control: Theory and Design, Nob Hill Publishing, 2009.

[19] L. Grüne, Economic receding horizon control without terminal constraints, Automatica 49 (3) (2013) 725 – 734.

[20] M. Ellis, J. Liu, P. Christofides, Economic Model Predictive Control, Springer, 2017.

[21] I. Prodan, E. Zio, F. Stoican, Fault tolerant predictive control design for reliable microgrid energy management under uncertainties, Energy 91 (2015) 20–34.

[22] A. Lefort, R. Bourdaisa, G. Ansanay-Alexb, H. Guéguen, Hierarchical control method applied to energy management of a residential house, Energy and Buildings 64 (2013) 53–61.

[23] A. van der Schaft, D. Jeltsema, Port-Hamiltonian systems theory: An introductory overview, Foundations and Trends in Systems and Control 1 (2-3) (2014) 173–378.

[24] T. Pham, I. Prodan, D. Genon-Catalot, L. Lefèvre, Power balancing in a DC microgrid elevator system through constrained optimization, in: 20th World Congress of the International Federation of Automatic Control, Vol. 50, Elsevier, 2017, pp. 19 – 24.

[25] A. van der Schaft, B. Maschke, Port-Hamiltonian system on graphs, SIAM Journal on Control and Optimization 51 (2) (2013) 906–937.

[26] J. Manwell, J. McGowan, Lead acid battery storage model for hybrid energy systems, Solar Energy 50 (5) (1993) 399–405.

[27] D. Lifshitz, G. Weiss, Optimal energy management for grid-connected storage systems, Optimal Control: Application and Methods 36 (4) (2015) 447–462.

[28] C. Desdouits, M. Alamir, V. Boutin, C. Pape, Multisource elevator energy optimization and control, in: Proceedings of the European Control Conference, Linz, Autria, 2015.

[29] D. Paire, M. Simoes, J. Lagorse, A. Miraoui, A real-time sharing reference voltage for hybrid generation power system, in: IEEE Industry Applications Society Annual Meeting, IEEE, Houston, TX, 2010, pp. 1–8.

[30] D. Zonetti, R. Ortega, A. Benchaib, Modeling and control of HVDC transmission systems from theory to practice and back, Control Engineering Practice 45 (2015) 133–146.

[31] J. Zhao, F. Dörfler, Distributed control and optimization in DC microgrids, Automatica 61 (2015) 18–26.

[32] T. Pham, Constrained optimization-based control for dc microgrids, Ph.D. thesis, Université Grenoble Alpes, France, tel-01762555 (2017).

[33] P. Kotyczka, L. Lefèvre, Discrete-Time Port-Hamiltonian Systems Based on Gauss-Legendre Collocation, in: 6th IFAC Workshop on Lagrangian and Hamiltonian Methods for Nonlinear Control, Vol. 51, Valparaíso, Chile, Elsevier, 2018, pp. 125 – 130.

[34] M. Duran, I. Grossmann, An outer-approximation algorithm for a class of mixed-integer nonlinear programs, Mathematical Programming 36 (1986) 307–339.

[35] I. Prodan, F. Stoican, S. Olaru, S. Niculescu, Enhancements on the Hyperplanes Arrangements in Mixed-Integer Programming Techniques, Journal of Optimization Theory and Applications 154 (2) (2012) 549–572.

[36] L. T. Biegler, V. M. Zavala, Large-scale nonlinear programming using ipopt: An integrating framework for enterprise-wide dynamic optimization, Computers & Chemical Engineering 33 (3) (2009) 575–582.

[37] M. Hovd, R. Braatz, Handling state and output constraints in MPC using timedependent weights, in: Proceedings of the IEEE American Control Conference, Vol. 3, IEEE, 2001, pp. 2418–2423.

[38] P. Christofides, R. Scattolini, D. M. noz de la Peña, J. Liu, Distributed model predictive control: A tutorial review and future research directions, Computers & Chemical Engineering 51 (2013) 21–41.

[39] J. Löfberg, YALMIP: A toolbox for modeling and optimization in MATLAB, in: IEEE International Symposium on Computer Aided Control Systems Design, IEEE, 2004, pp. 284–289.

[40] A. Wächter, An interior point algorithm for large-scale nonlinear optimization with applications in process engineering, Ph.D. thesis, Carnegie Mellon University (2002).

[41] J. B ungelera, E. Cattaneoa, B. Riegela, D. U. Sauerb, Advantages in energy efficiency of flooded lead-acid batteries when using partial state of charge operation, Journal of Power Sources 375 (2018) 53–58.

[42] E. Hairer, C. Lubich, G. Wanner, Geometric Numerical Integration: Structure-Preserving Algorithms for Ordinary Differential Equations, Springer, 2006.